Room-temperature direct-bandgap photoluminescence from strain-compensated Ge/SiGe multiple quantum wells on silicon*

Hu Wei-Xuan(胡炜玄), Cheng Bu-Wen(成步文)†, Xue Chun-Lai(薛春来), Zhang Guang-Ze(张广泽), Su Shao-Jian(苏少坚), Zuo Yu-Hua(左玉华), and Wang Qi-Ming(王启明)

State Key Laboratory on Integrated Optoelectronics, Institute of Semiconductors, Chinese Academy of Sciences, Beijing 100083, *China*

(Received 23 March 2011; revised manuscript received 15 September 2011)

Strain-compensated $Ge/Si_{0.15}Ge_{0.85}$ multiple quantum wells were grown on an $Si_{0.1}Ge_{0.9}$ virtual substrate using ultrahigh vacuum chemical vapor deposition technology on an n^+-Si(001) substrate. Photoluminescence measurements were performed at room temperature, and the quantum confinement effect of the direct-bandgap transitions of a Ge quantum well was observed, which is in good agreement with the calculated results. The luminescence mechanism was discussed by recombination rate analysis and the temperature dependence of the luminescence spectrum.

Keywords: Ge, multiple quantum wells, strain compensated

PACS: 78.55.–m, 73.61.Cw **DOI:** 10.1088/1674-1056/21/1/017805

1. Introduction

It was predicted in the early 1990s that silicon-based optoelectronics integration would be a reality in the future.[1] Optoelectronic integration techniques merge the function of optical communication devices and microelectronic devices into one chip. Because of its high compatibility with Si complementary metal oxide semiconductor processes and the 1550 nm light emission and absorption from direct band-to-band transition, Ge has become a promising candidate for monolithically integrated Si-based optoelectronics integration. For instance, a Ge-on-Si p–i–n photodetector with high responsibility and low dark current working at the NIR region has been demonstrated,[2] and a high gain Ge avalanche photodetector with low noise has been reported.[3,4] Despite the low efficiency under larger injection, an electrically pumped Ge light emission diode,[5,6] and even an optically pumped Ge laser[7] working at room temperature, have also been reported.

The Ge/SiGe quantum-well structure can improve the performance of present devices, and also has great potential application in new optoelectronic devices. By using the compositional graded SiGe buffer layer or the "low-temperature/high-temperature" strategy,[8,9] a Ge layer and a Ge/SiGe quantum well with high Ge content can be grown on an Si substrate with high quality and become available in device applications. The quantum confinement effect in the Ge/SiGe structure has been applied in waveguide photodetectors[10] and Ge/SiGe modulators based on the quantum-confined stark effect.[11] Moreover, the quantum confinement effect has been widely used to improve the performance of compound semiconductor light emitting devices.[12] It may also be valid to confine the carriers during the light emission of Ge, and emission efficiency enhancement is expected. Thus, studies of the quantum confinement effect and the photoluminescence of Ge/SiGe quantum wells are important.

In this paper, we grew strain-compensated $Ge/Si_{0.15}Ge_{0.85}$ multiple quantum wells (MQWs) on a $Si_{0.1}Ge_{0.9}$ layer on the Si(001) substrate to investigate the quantum confinement effect of $Ge/Si_{0.15}Ge_{0.85}$ quantum wells (QWs). A strain-balanced structure was introduced to improve the material quality. Direct-bandgap photoluminescence (PL) mea-

*Project supported by the National Natural Science Foundation of China (Grant Nos. 61036003, 61176013, 61177038, and 60906035), and the High Technology Research and Development Program of China (Grant No. 2011AA010302).

†Corresponding author. E-mail: cbw@semi.ac.cn

© 2012 Chinese Physical Society and IOP Publishing Ltd

surements were performed at room temperature, and the quantum confinement effect of the Ge QW was observed, which agrees well with the calculated results. The luminescence mechanism was discussed by recombination rate analysis and the temperature dependence of the luminescence spectrum.

2. Experimental procedures

The n^+Si (001) substrate, with a resistivity of 0.001 Ω·cm, was cleaned using an improved RCA wet-chemical cleaning recipe, i.e. using H_2O_2: H_2SO_4=1:4, H_2O_2: NH_4OH: H_2O=2:1:5, HF: H_2O=1:10, H_2O_2: HCl: H_2O=7:1:2 solutions, sequentially. Before growing in the cold wall ultrahigh vacuum chemical-vapor-deposition (UHVCVD) system, the substrate was degassed at 300 °C in the pretreatment chamber and deoxided in the growth chamber by heating to 930 °C for 5 min. The base pressure of the system was 1×10^{-7} Pa. Then, the deposition of a 50 nm thick Ge buffer layer occurred at 290 °C with a flow of 8 sccm pure GeH_4. Next, a 700 nm $Si_{0.1}Ge_{0.9}$ layer was grown at 600 °C on the 50 nm Ge buffer layer with a flow of 8 sccm pure GeH_4 and 0.6 sccm pure Si_2H_6. After that, 10 periods of $Ge/Si_{0.15}Ge_{0.85}$ strain-compensated QWs were grown on the 700 nm $Si_{0.1}Ge_{0.9}$. The thicknesses of the Ge well and $Si_{0.15}Ge_{0.85}$ barrier were 10 and 18 nm for sample 1, and 18 and 27 nm for sample 2, respectively. Finally, the QWs were capped by a 180 nm thick $Si_{0.1}Ge_{0.9}$ top layer. For the sake of comparison, three samples of $Si_{1-x}Ge_x$ films were also grown on the n^+-Si(001) substrate ($x = 0.85$ for sample 3, $x = 0.9$ for sample 4 and $x = 1$ for sample 5) using the "low-temperature/high-temperature" strategy with a 50 nm thick Ge buffer layer. The thicknesses of the $Si_{1-x}Ge_x$ layer were 850, 700 and 1000 nm for samples 3–5, respectively. The schematic cross sectional views of these five samples are shown in Fig. 1. Atomic force measurements (AFM) were performed to evaluate the material quality of all the samples. The details of the material growth can be seen in our previous work.[8]

X-ray diffraction (XRD) measurements along the (004) direction were performed using the Cu-$k_{\alpha1}$ ($\lambda = 0.15406$ nm) X-ray source to evaluate the structure and material quality of the $Ge/Si_{0.15}Ge_{0.85}$ MQWs for samples 1 and 2. XRD measurements along the (004) and (224) directions for samples 3–5 were also carried out to estimate the strain status and Ge fractions of the $Si_{1-x}Ge_x$ layer. The luminescence of samples 1–5 were studied by PL measurements with LabRam HR 800 Raman instrumentation at room temperature. During the measurements, the samples were excited with a 488 nm laser and the emitted light was detected by an InGaAs photodetector within the range 0.775–1.24 eV.

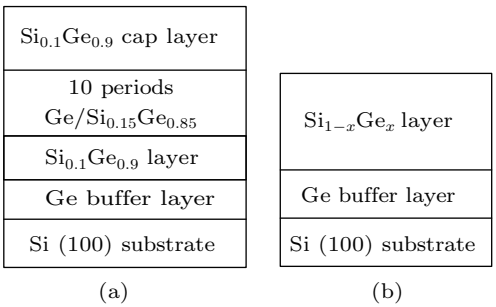


Fig. 1. The cross sectional views of samples 1–5. The Ge buffer layers are 50 nm thick for samples 1–5. (a) For samples 1 and 2, the thicknesses of the $Si_{0.1}Ge_{0.9}$ layers and the cap layers are 700 and 180 nm, respectively; for sample 1, the thicknesses of the Ge and $Si_{0.15}Ge_{0.85}$ layers of the quantum wells are 10 and 18 nm, respectively; while for sample 2, these thicknesses are 18 and 27 nm, respectively. (b) For samples 3–5, the thicknesses of the $Si_{1-x}Ge_x$ layers are 850, 700 and 1000 nm, respectively; and the Ge compositions are $x = 0.85$ for sample 3, $x = 0.9$ for sample 4 and $x = 1$ for sample 5.

3. Results and discussion

The deposition of Ge on an Si substrate is a typical example of Stranski–Krastanow growth.[13] Because of the 4.2% lattice mismatch, when the thickness of the Ge layer is beyond the critical thickness (about four monolayers),[14,15] the growth mode tends to transfer from two-dimensional growth to island growth. In this case, it is energetically favorable to release the strain energy by forming misfit dislocations at the Ge/Si interface and threading dislocations through the Ge layer. Nevertheless, the transition from two-dimensional growth to island growth can be avoided by introducing the Ge buffer layer at low temperature.[16,17] At low temperature, the Ge adatom on the Si surface does not have enough energy to move and form an island. Thus, we can obtain a high-quality Ge layer and $Si_{1-x}Ge_x$ film with a high Ge fraction. The surface morphology of samples 1–5 measured by AFM are shown in Fig. 2.

The experimental and simulated XRD rocking curves along the (004) direction of Ge/SiGe MQWs (samples 1 and 2) are shown in Fig. 3. A series of satellite peaks can be seen, which indicate high crystal quality and an abrupt interface between the Ge and $Si_{0.15}Ge_{0.85}$ layer in the QWs. The diffraction

peak of the relaxed $Si_{0.1}Ge_{0.9}$ layer is overlapped by the zero-order satellite peak of the $Ge/Si_{0.15}Ge_{0.85}$ QWs, which supports the strain-compensated structure. This strained compensated QW structure offers a number of advantages to guarantee the material quality by balancing the tensile and compressive strain.[18] The average angular separation between adjacent satellites is in good agreement with the thickness of the period $Ge/Si_{0.15}Ge_{0.85}$ QWs. XRD measurements along the (004) and (224) directions of samples 3–5 were also performed (the results are not shown here). The strain and Ge fraction are calculated by comparing the XRD spectra along the (004) and (224) directions. The results of sample 4 show that the 700 nm $Si_{0.1}Ge_{0.9}$ on a 50 nm Ge buffer layer is under 0.07% tensile strain. By using the strain data of the 700 nm $Si_{0.1}Ge_{0.9}$ on the 50 nm Ge layer, the strain of the Ge and $Si_{0.15}Ge_{0.85}$ layer of the QWs was calculated to be 0.33% compressive strain and 0.27% tensile strain, respectively, of samples 1 and 2.

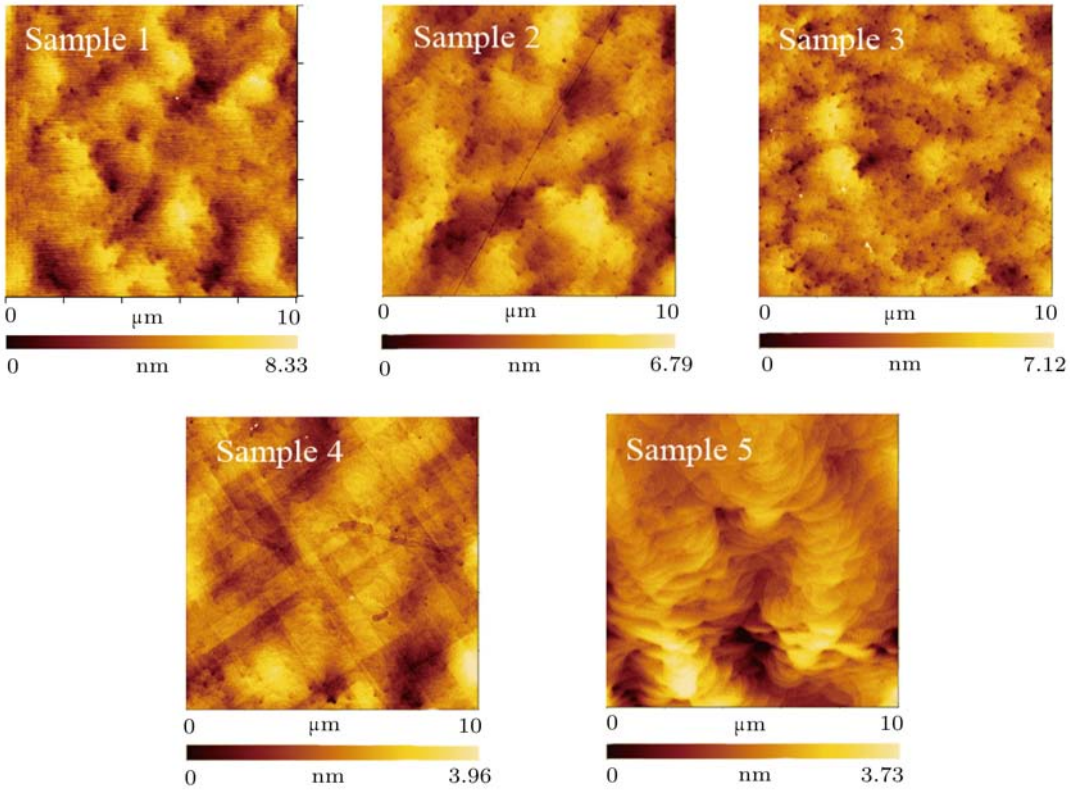


Fig. 2. (colour online) AFM images of samples 1–5. The RMS roughnesses of samples 1–5 are 1.26, 1.08, 0.97, 0.60 and 0.57 nm, respectively.

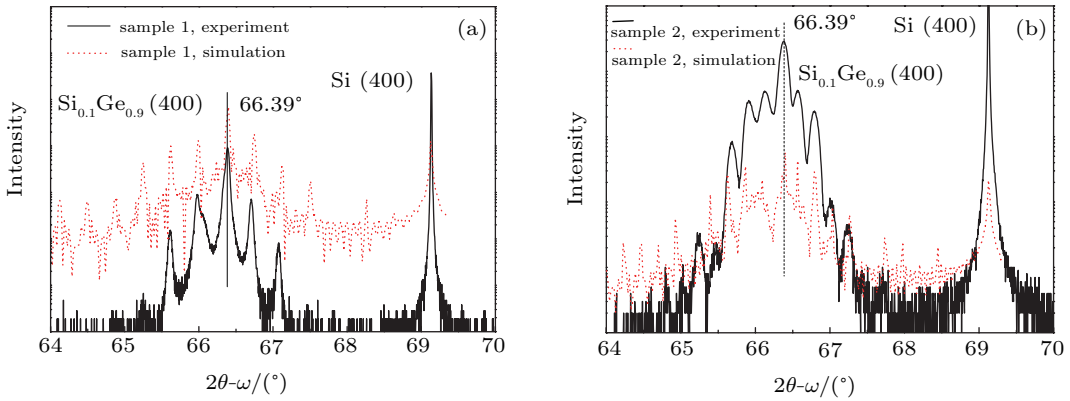


Fig. 3. (colour online) XRD rocking curves of the strain-compensated Ge/SiGe quantum wells along the (400) direction of sample 1 (a) and sample 2 (b). The solid line is the measurement result and the dotted line is the simulation result.

Using the strain status of each layer calculated above, the band edge diagrams of the MQWs of samples 1 and 2 are calculated using the deformation potentials theory, with linear interpolation of the deformation potentials and direct bandgap of SiGe between Si and Ge.[19,20] The results are shown in Fig. 4. As can be seen, the conduction bands at

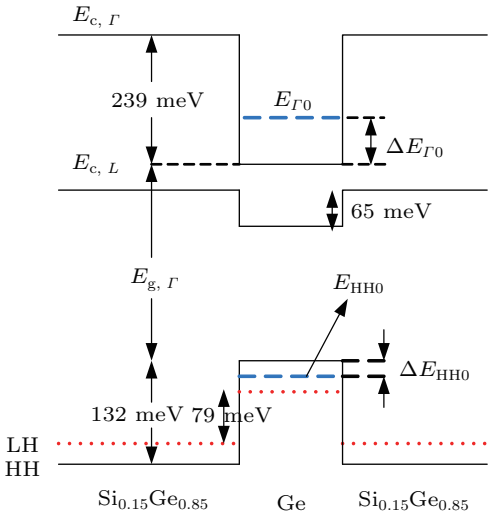


Fig. 4. (colour online) Band edge diagrams of samples 1 and 2. $E_{c,\Gamma}$ and $E_{c,L}$ are the conduction band minima at Γ point and L point, respectively. LH and HH are the valence band maxima of the light hole and the heavy hole, respectively, and the band discontinuities are shown in units of meV. $E_{\Gamma 0}$ and E_{HH0} are the ground states of electrons and heavy holes at Γ point, respectively. For sample 1, $\Delta E_{\Gamma 0} = 43$ meV, $\Delta E_{HH0} = 8$ meV, and for sample 2, $\Delta E_{\Gamma 0} = 18$ meV, $\Delta E_{HH0} = 3$ meV. The direct bandgap of the Ge well is $E_{g,\Gamma} = 0.821$ eV for samples 1 and 2.

the L point and Γ point of the reciprocal space both indicate type-I band alignment. The deformation potentials used in the calculations can be seen in Refs. [17] and [18]. The heavy hole band is higher than the light hole band in the Ge well under compressed strain. The band discontinuities of the light hole, heavy hole and electron at the Γ point are calculated to be 79, 132, and 239 meV, respectively. The conduction band discontinuity is only 65 meV at the L point. The direct bandgap of the Ge well was calculated to be $E_{g,\Gamma} = 0.821$ eV. Comparing with the 0.8 eV direct bandgap of bulk Ge, the 21-meV blue shift of the direct bandgap was induced by the 0.33% compressive strain of the Ge well. At the Γ point, discrete energy levels are formed in the Ge well because of the quantum confinement effect. Using the finite potential well model, the ground energy state of electron $E_{\Gamma 0}$ is calculated to be 43 meV on the top of the conduction band minimum for a 10-nm thick Ge well (sample 1), while this value is 18 meV for an 18-nm thick Ge well (sample 2). The ground energy state of heavy hole E_{HH0} is 8 meV below the valence band maximum for the 10-nm thick Ge well (sample 1), while this value is 3 meV for the 18-nm thick Ge well (sample 2).

Radiative recombination from the energy level $E_{\Gamma 0}$ to E_{HH0} was observed in the PL spectrum in Fig. 5 of samples 1 and 2. In the PL spectra of all the samples, the water absorption range from 0.886 to 0.919 eV is shown as a rectangle. The intensity of the PL spectra were normalized and then moved to separate from each other. The 0.866 eV luminescence peak of sample 1 and the 0.834 eV luminescence peak of sample 2 source from the direct bandgap transition of the Ge layer in the $Ge/Si_{0.15}Ge_{0.85}$ QWs at the Γ point, from the ground state of the conduction band $E_{\Gamma 0}$ to the ground state of the heavy hole E_{HH0}.[21] Theoretically, the transition energy from $E_{\Gamma 0}$ to E_{HH0} was calculated to be 0.872 and 0.842 eV for samples 1 and 2, respectively, according to the band edge diagram in Fig. 3. The calculated transition energies of 0.872 and 0.842 eV are in good agreement with the observed 0.866 and 0.834 eV for samples 1 and 2, respectively. The difference between the calculated and observed transition energy of sample 1 (5 meV = 0.87 eV − 0.866 eV) and sample 2 (7 meV = 0.841 eV − 0.834 eV) were mainly caused by the diffusion between the Ge well and the $Si_{0.15}Ge_{0.85}$ barrier.

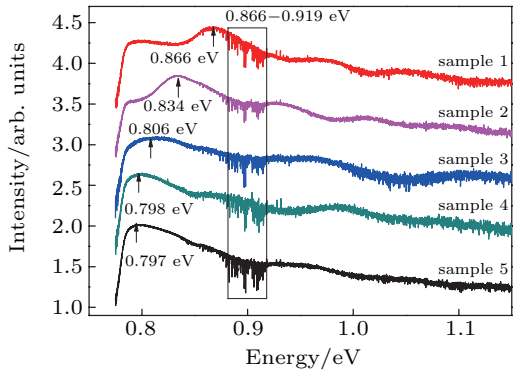


Fig. 5. (colour online) The PL spectra of samples 1–5 ranging from 0.775 to 1.24 eV at room temperature. The water vapor absorption range from 0.886 to 0.919 eV is shown in a rectangle. The intensity of the PL spectra were normalized and then moved to separate from each other.

In the conduction band of bulk Ge, the L point is lower than the Γ point for 140 meV ($E_\Gamma - E_L =$

140 meV, where E_Γ, E_L are the energies of the conduction band minima at the Γ point and the L point, respectively). In addition, the effective mass of the density of states of the Γ point $m_{\Gamma,\mathrm{DOS}}$ is much smaller than that of the L point $m_{L,\mathrm{DOS}}$ ($m_{\Gamma,\mathrm{DOS}} = 0.038m_\mathrm{e}$, $m_{L,\mathrm{DOS}} = 0.216m_\mathrm{e}$, where m_e is the rest mass of the electron). For the two reasons mentioned above, electrons at the Γ point tend to be scattered into the L point with a high probability, which prevents radiative recombination. Nevertheless, in the equilibrium state, $N_\Gamma \approx N_L \exp[(E_L - E_\Gamma)/k_\mathrm{B}T]\,(m_{\Gamma,\mathrm{DOS}}/m_{L,\mathrm{DOS}})^{3/2} \approx 0.001N_L$, where N_Γ and N_L are the electron numbers at the Γ point and the L point, respectively.[22,23] Moreover, the radiative recombination rate of the Γ point is much higher than that of the L point.[5] With the electrons and the high radiative recombination rate of the Γ point, the direct bandgap transition can still be observed.

The luminescence peak energies under temperatures of 30 °C, 50 °C, 70 °C and 90 °C of sample 1 (0.866 eV) and sample 2 (0.834 eV) are shown in Fig. 6. The variations of the luminescence peak under different temperatures prove the band-to-band transition mechanism, in other words, the luminescence is not emitted from extraneous sources (such as impurity, interface states and glass windows), because luminescence temperature dependence is a feature of the band-to-band transition of semiconductors.

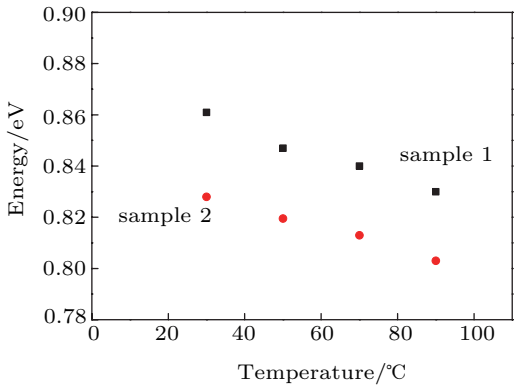


Fig. 6. (colour online) The luminescence peak energies of sample 1 (0.866 eV) and sample 2 (0.834 eV) under temperatures of 30 to 50 °C, 70 °C and 90 °C, respectively. The rectangular and circular scatter data points are the measurement results of samples 1 and 2, respectively. The variations in luminescence peak under different temperatures support the band-to-band transition mechanism.

For the sake of comparison, the PL measurements of samples 3–5 were also performed. As shown in Fig. 5, the 0.806 eV peak of sample 3 and the 0.798 eV peak of sample 4 are from the direct bandgap transition of the 50 nm Ge buffer layer. For sample 5, the 0.797 eV peak is from the direct bandgap transition of the Ge layer. The difference between the energies of these three peaks may be caused by the different strain status.[20,21] Although the Ge luminescence peaks of samples 3–5 around 0.8 eV may be affected by detector falloff, the direct bandgap radiative recombination mechanism of Ge has been proved in our previous work,[5] via the blue-shift of luminescence peak energy and the emission power under different injection levels. The luminescence peak around 0.866 eV of sample 1 or 0.834 eV of sample 2 was not observed in the PL spectra of samples 3–5, indicating that the luminescence at 0.866 eV of sample 1 and 0.834 eV of sample 2 are not emitted from the Ge buffer layer, the $Si_{0.1}Ge_{0.9}$ layer or the $Si_{0.15}Ge_{0.85}$ barrier.

4. Conclusions

We have successfully grown high-quality strain-compensated $Ge/Si_{0.15}Ge_{0.85}$ MQWs. The direct-bandgap transitions at 0.866 and 0.834 eV for 10 and 18 nm Ge QWs, respectively, were observed at room temperature. The blue shift of the direct bandgap transition of Ge induced by the quantum confinement effect agrees well with the calculated result. Recombination rate analysis supports the direct bandgap radiative recombination mechanism, and the temperature dependence of the luminescence peak energy proves the band-to-band transition mechanism. The quantum confinement effect of the Ge/SiGe MQWs is expected to be applied in Si-based optoelectronic devices.

References

[1] Soref R and Fellow L 2006 *IEEE J. Sel. Top. Quantum Electron.* **12** 1678

[2] Xue H Y, Xue C L, Cheng B W, Yu Y D and Wang Q M 2009 *Chin. Phys.* B **18** 2542

[3] Kang Y M, Liu H D, Morse M, Paniccia M J, Zadka M, Litski S, Sarid G, Pauchard A, Kuo Y H, Chen H W, Zaoui W S, Bowers J E, Beling A, McIntosh D C, Zheng X G and Campbell J C 2009 *Nature Photonics* **3** 59

[4] Assefa S, Xia F N and Vlasov Y A 2010 *Nature* **464** 80

[5] Hu W X, Cheng B W, Xue C L, Xue H Y, Su S J, Bai A Q, Luo L P, Yu Y D and Wang Q M 2009 *Appl. Phys. Lett.* **95** 092102

[6] Sun X C, Liu J F, Kimerling L C and Michel J 2009 *Opt. Lett.* **34** 1198

[7] Liu J F, Sun X C, Aguilera R C, Kimerling L C and Michel J 2010 *Opt. Lett.* **35** 679

[8] Cheng B W, Xue H Y, Hu D, Han G Q, Zeng Y G, Bai A Q, Xue C L, Luo L P, Zuo Y H and Wang Q M 2008 *Proceedings of the Fifth IEEE International Conference on Group IV Photonics* September, Sorrento (Italy) p. 140

[9] Halbwax M, Bouchier D, Yam V, Débarre D, Nguyen L H, Zheng Y, Rosner P, Benamara M, Strunk H P and Clerc C 2005 *J. Appl. Phys.* **97** 064907

[10] Fidaner O, Okyay A K, Roth J E, Schaevitz R K, Kuo Y H, Saraswat K C, Harris J S and Miller D A B 2007 *IEEE Photon. Technol. Lett.* **19** 1631

[11] Chaisakul P, Morini D M, Isella G, Chrastina D, Roux X L, Gatti E, Edmond S, Osmond J, Cassan E and Vivien L 2010 *Opt. Lett.* **35** 2913

[12] Li S M, Song S M, Lü Y B, Wang A F, Wu A L and Zheng W M 2009 *Acta Phys. Sin.* **58** 4936 (in Chinese)

[13] LeThanh V, Yam V, Meneceur N, Boucaud P, Débarre D and Bouchier D 2001 *Mater. Phys. Mech.* **4** 94

[14] Varga K, Wang L G, Pantelides S T and Zhang Z Y 2004 *Surface Science* **562** L225

[15] People R and Bean J C 1985 *Appl. Phys. Lett.* **47** 322

[16] Shin K W, Kim H W, Kim J, Yang C, Lee S and Yoon E 2010 *Thin Solid Films* **518** 6496

[17] Hartmann J M, Papon A M, Destefanis V and Billon T 2008 *J. Cryst. Growth* **310** 5287

[18] Ekins-Daukes N J, Kawaguchi K and Zhang J 2002 *Crystal Growth & Design* **2** 287

[19] Liu J F, Cannon D D, Wada K, Ishikawa Y, Danielson D T, Jongthammanurak S, Michel J and Kimerling L C 2004 *Phys. Rev.* B **70** 155309

[20] van de Walle C G 1989 *Phys. Rev.* B **39** 1871

[21] Haynes J R 1955 *Phys. Rev.* **98** 1866

[22] Liu J F, Sun X C, Pan D, Wang X X, Kimerling L C, Koch T L and Michel J 2007 *Opt. Express* **15** 11272

[23] Ishikawa Y, Wada K, Cannon D D, Liu J F, Chiao L H and Kimerling L C 2003 *Appl. Phys. Lett.* **82** 2044